Mathematical Biosciences 246 (2013) 47–54

Contents lists available at ScienceDirect

Mathematical Biosciences

journal homepage: www.elsevier.com/locate/mbs

Extension and verification of the SEIR model on the 2009 influenza A (H1N1) pandemic in Japan

Masaya M. Saito [a,*], Seiya Imoto [b], Rui Yamaguchi [b], Hiroki Sato [c], Haruka Nakada [d], Masahiro Kami [d], Satoru Miyano [b], Tomoyuki Higuchi [a]

[a] The Institute of Statistical Mathematics, 10-3 Midoricho, Tachikawa, Tokyo 190-8562, Japan
[b] Human Genome Center, Institute of Medical Science, University of Tokyo, 4-6-1 Shirokanedai, Minato-ku, Tokyo 108-8639, Japan
[c] Department of Medical Informatics, National Defense Medical College Hospital, 3-2 Namiki, Tokorozawa City, Saitama 359-8513, Japan
[d] Division of Social Communication Systems for Advanced Clinical Research, Institute of Medical Science, University of Tokyo, 4-6-1 Shirokanedai, Minato-ku, Tokyo 108-8639, Japan

ARTICLE INFO

Article history:
Received 20 December 2010
Received in revised form 20 August 2013
Accepted 23 August 2013
Available online 4 September 2013

Keywords:
Data assimilation
Influenza pandemic simulation
SEIR model

ABSTRACT

In order to understand the evolution of the 2009 influenza A (H1N1) pandemic within local regions of Japan, we studied the significance of regional migration between these regions. For this purpose, we have employed an extended SEIR model to describe the immigration of infected people and the stochastic variation of the infectious efficiency. We then applied a data assimilation technique in order to study how the agreement of the simulation results with the observed data depends on the presence/absence of immigration and the degree of variation of the infectious efficiency. Reproducibility is evaluated by log-likelihood values. The log-likelihood does not indicate the significance of immigration. Although there are multiple waves in the time course of the number of reported infected individuals, these waves could be explained by the stochastic nature of infectious events.

1. Introduction

In 2009, a novel swine-origin influenza A (H1N1) virus caused worldwide outbreaks of influenza. From 28 April, the Japanese government carried out onboard quarantine inspections at Narita International Airport (Chiba Prefecture, in the Kanto area) in order to prevent or delay the entry of infected people. Three people infected with the novel influenza virus, who were detected by the inspections on 8 May, were confirmed by RT-PCR. These were the first pandemic influenza cases detected in Japan. However, another three cases were detected on 16 May in Kobe City (Hyogo Prefecture, in the Kansai area); these were the first confirmed domestic cases. The locations of the Kansai and Kanto areas of Japan are shown in Fig. 1.

Because the infected individuals had no history of overseas travel, these cases should be considered to be secondary due to primary cases that either had not been detected by the onboard quarantine inspections or had entered Japan before the inspection procedure began. An assessment [1] of the detection rate of the border quarantine indicates that the effectiveness of the quarantine was limited. Positive diagnoses continued through 24 July, by which time 4,986 cases had been confirmed [2]. The indigenous infection was judged to be already sustainable by that day, and the number of infected people is estimated to have peaked in November [2].

The progress of the epidemic up to 24 July is summarized as follows: The first epidemic wave in Kansai preceded the epidemic wave in Kanto, but after the wave hit Kanto, a second wave hit Kansai. In addition, it was reported in a white paper [3] that Kobe City conducted preventive school closures immediately after the discovery of the first domestic case and stayed on special alert until 28 May. Therefore, it is a plausible scenario that the first wave in Kansai died out due to the efforts of the local government, but the surviving influenza virus in Kanto brought another wave of the epidemic to Kansai. In this paper, we study whether this scenario is statistically supported by the reported confirmed cases. To do this, we introduce an extended version of the susceptible-exposed-infected-removed (SEIR) model in which the degree of exchange of infected individuals between Kansai and Kanto is controlled by parameters ε_{ij}. The proposed scenario is considered to be plausible if the likelihood value is significantly larger with some nonzero ε_{ij} than it is for $\varepsilon_{ij} = 0$.

Studies of the effect of the mixing of different populations between cities go back to 1985 [4]. This study showed that the Hong Kong flu in 1968 could be reconstructed by using a model involving 52 cities connected by airline routes. A similar study that focused on an endemic forecast for Europe was also carried out [5]; nine cities connected by airlines were considered. The connectivity of populations also plays an important role in the spread of infection at a smaller scale. Ferguson et al. [6] chose Thailand as a target area

* Corresponding author. Tel.: +81 50 5533 8582; fax: +81 42 526 4335.
E-mail address: saitohm@ism.ac.jp (M.M. Saito).

0025-5564/$ - see front matter © 2013 Elsevier Inc. All rights reserved.
http://dx.doi.org/10.1016/j.mbs.2013.08.009

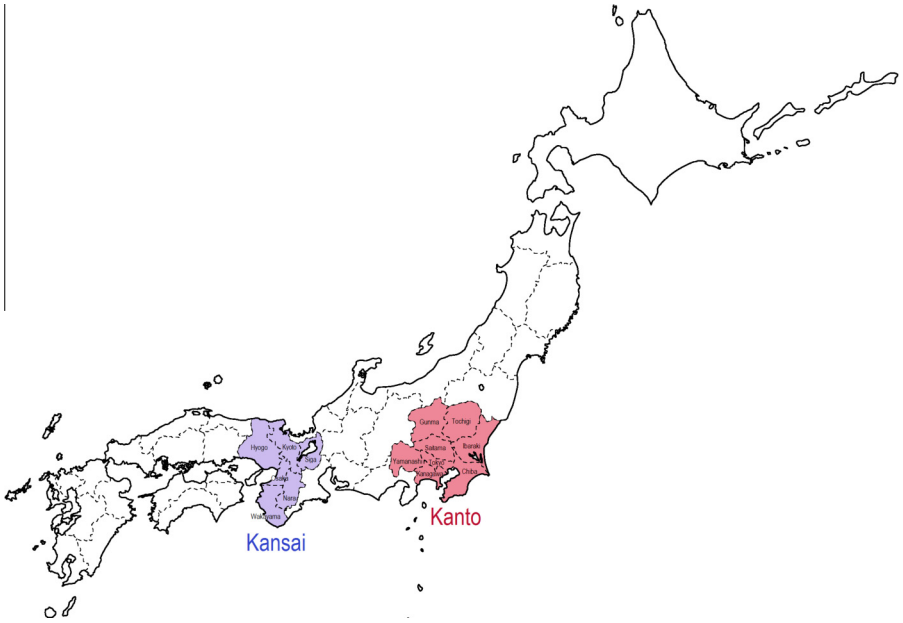

Fig. 1. Locations of the Kansai and Kanto areas of Japan.

and modelled a set of groups (such as schools and homes) in which members contacted each other. In this model, depending on their roles, individuals could belong to multiple groups, which then described their mobility (for example, between their home and workplace). Longini et al. [7] dealt with the same target using a different modelling approach, in which each individual belonged to a single group, but in which distance transmission from any individual was allowed. Various ways of modelling infectious transmission between multiple populations was reviewed by Riley [8].

A data assimilation technique, which uses observations to improve a simulation model, is used to obtain the maximal likelihood value for the given ε_{ij} and to estimate the parameters. This technique was developed in the fields of oceanography and meteorology [9], but it is now applied in various research fields, including biology [10]. The main applications of data assimilation are estimating the parameters, making forecasts, and estimating the simulation variables. In the case of our extended model, the simulation variables consist of the populations of susceptible and infected people and the infectious efficiency. It is important to study how the infectious efficiency varies over the time as well as its uncertainty in order to design effective policy measures.

This paper is organized as follows. In Section 2, the SEIR model is extended to include a time-varying infectious efficiency and the immigration of infected individuals. In Section 2.1, the original SEIR model is introduced. The observed time-course profiles are explained in Section 2.2, and the necessary extensions for adapting the SEIR model to these profiles are presented in Section 2.3. In Section 2.4, a state-space model is introduced as a framework for the data assimilation technique. The results of simulations from the original and our extended SEIR models are presented in Section 3. Comparing the simulation results of these two models to the observed data, we evaluate the significance of the immigration of infected people. Section 4 presents a discussion and our concluding remarks.

2. Methods

2.1. The SEIR model

The susceptible-infected-removed (SIR) model and the SEIR model [11], which was developed from it, are widely used in epidemic simulations. The SEIR model separates the population of a region into four compartments, *susceptible*, *exposed*, *infected*, and *removed*, and simulates the time evolution of each of these subpopulations. Let S_i, E_i, I_i, and R_i be the populations of these compartments in region $i : i = 1$ (Kansai) and $i = 2$ (Kanto). Then, the SEIR model is given by

$$\dot{S}_i = -\beta_i \left(\frac{I_i}{N_i}\right) S_i, \tag{1}$$

$$\dot{E}_i = \beta_i \left(\frac{I_i}{N_i}\right) S_i - \alpha_i E_i, \tag{2}$$

$$\dot{I}_i = \alpha_i E_i - \gamma I_i, \tag{3}$$

$$\dot{R}_i = \gamma I_i, \tag{4}$$

where $\dot{A} \equiv dA/dt$ and the unit of time is one day. In any solution of these equations, $S_i + E_i + I_i + R_i \equiv N_i$ is constant, which means that the population in the region is conserved. Although both the exposed and the infected individuals are infected, they are distinguished by the absence/presence of their ability to infect other people. The constant $1/\alpha_i$ describes the time scale during which a newly infected individual acquires the ability to infect others. Similarly, the constant $1/\gamma$ describes the expected time to recovery. The number of newly infected people due to one infected individual per day is given by $\beta_i \cdot (S_i/N_i)$. Hence, $\beta_i \cdot (S_i(t)/N_i) \cdot (1/\gamma) \equiv \mathcal{R}_i(t)$ gives the expected number of infected people due to one infected individual. In the early stage of an epidemic, $I_i(t), E_i(t) \approx 0$ and $S_i(t) \approx N_i$, and hence the constant $\mathcal{R}_{i,0} \equiv \beta_i/\gamma$ is used to predict whether the number of infected people will increase or decrease. We notate the *basic reproduction number* as $\mathcal{R}_{i,0}$, and $\mathcal{R}_i$ is simply called the *reproduction number*. For further interpretation of the SEIR model, see [12,13]. By combining Eqs. (2) and (3), we find that $I_i + E_i$ increases if $\mathcal{R}_i > 1$ and decreases if $\mathcal{R}_i < 1$. Moreover, since Eq. (1) is always negative or zero, $\mathcal{R}_i$ ($\propto S_i$) monotonically decreases as t increases. This implies that there is only a single peak of the infectious population for any solution of the SEIR model.

2.2. Data generation process

The National Institute of Infectious Diseases provided time-course data for the confirmed infected individuals from 21 May to 25 July 2009 (66 time points) in each of the 47 prefectures of Japan. Let $J_i^{\mathrm{obs}}[t]$ be the number of infected people confirmed on day t in region i. We note that the values of $J_i^{\mathrm{obs}}[t]$ are close to zero in almost all prefectures except for the prefectures in the Kansai and Kanto regions. Therefore, we focused on the simulation of indigenous transmission of pandemic influenza in these areas. Because the numbers of confirmed infected people in the individual prefectures was not large enough for a macro simulation in the period of interest, we considered the six prefectures that include Osaka as the Kansai region (region 1), with a total population N_1 of 20,839,000. The eight prefectures that include Tokyo were considered to be the Kanto region (region 2), with a total population N_2 of 42,848,000. We denoted the number of confirmed cases in each of the regions by $J_1^{\mathrm{obs}}[t]$ and $J_2^{\mathrm{obs}}[t]$. Fig. 2 shows the time-course profiles of $J_1^{\mathrm{obs}}[t]$ (blue dots) and $J_2^{\mathrm{obs}}[t]$ (red dots).[1]

As can be seen, in Kansai, one epidemic wave ended around the end of May, and another epidemic wave began around 20 June, whereas the beginning of the epidemic wave in Kanto occurs around June 10. These features suggested to us the following scenario. At first, because $\mathcal{R}_1$ became less than unity, the first endemic in Kansai moved toward termination. Before this epidemic wave ended, however, some infected people from Kansai moved to Kanto, causing an endemic there. Then, $\mathcal{R}_1$ becomes greater than unity and some infected individuals from Kanto move to Kansai and cause a second endemic wave in Kansai. For this scenario, we assume a continuation of the trend in the number of patients that is reported in Fig. 2. However, since the total number of patients in this report is small, some local outbreaks may erroneously appear to be part of a global trend. In particular, the downward trend in Kansai toward the end of May might be a local event. To examine this possibility, we observe the number of patients on a smaller scale. Table 1 shows the cumulative number of age-specific confirmed cases in several cities in the Kansai region as well as the number in the Kanto region, for the period up to 31 May. The patients are predominantly in the age group from 10 to 19 years old, and a significant number of these patients are reported in Kobe and other cities in the Kansai region. This suggests that there were multiple transmission chains in Kansai, and that they were mainly in the schools. Although we do not have clear evidence that the reproduction number was successfully reduced to below unity, school closures were implemented immediately after the discovery of the first domestic case in Kobe City, and that may have been sufficient to decrease transmission. On the other hand, few patients were reported before the end of May. In this study, we will assume that the actual number of patients was proportional to the reported number.

For simplicity, we assume that the number of newly confirmed cases per unit time is proportional to the number of persons who change their state from the exposed to the infected, namely proportional to αE. In words, it is assumed that the appearance of symptom coincides with the acquisition of infectiousness, and surveillance activities detect diseases in a constance efficiency. The counterpart of $J^{\mathrm{obs}}[t]$ in the SEIR model is then given by,

$$J_i[t] = \int_{t-1}^{t} \alpha_i E_i(\tau) d\tau,$$

where we $A[t]$ denotes that quantity A is defined for discrete, observed points in time. To combine this with the SEIR model, we use the differential form

[1] For interpretation of color in Fig. 2, the reader is referred to the web version of this article.

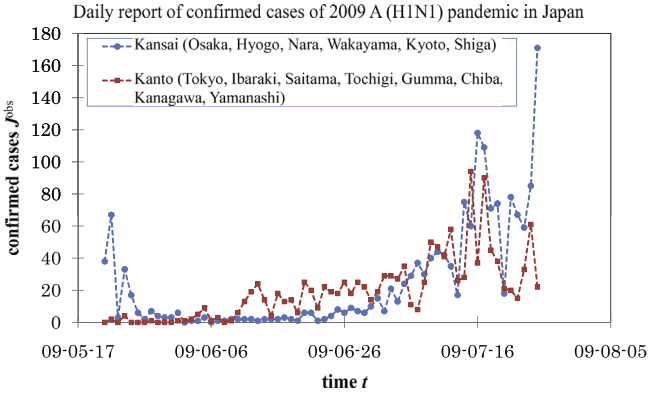

Fig. 2. Observed time course of recognized infectious populations J_i^{obs} in Kansai ($i = 1$) and Kanto ($i = 2$).

Table 1
Cumulative number of confirmed cases in the whole Kanto region and several cities in Hyogo and Osaka (prefectures in Kansai region), up to 31 May.

age	–	0s	10s	20s	30s	40s	50s	60–
Kanto	–	0	3	3	2	0	0	0
Osaka	Osaka	1	15	4	2	1	0	0
	Takatsuki	0	13	0	0	3	1	0
	Sakai	0	1	0	0	0	0	0
	the rest	2	105	4	1	4	0	0
Hyogo	Kobe	6	84	8	2	2	3	1
	Himeji	0	1	0	0	0	0	0
	Amagasaki	2	12	2	1	1	0	2
	Nishimomiya	0	2	0	0	0	0	0
	the rest	4	51	4	4	2	1	0

$$\dot{J}_i = \alpha_i E_i. \tag{5}$$

A constant related to detection rate is omitted by appropriately scaling the parameters and the initial conditions of the SEIR model.

2.3. Extension of the model

We extend the SEIR model as follows. First, we allow the migration of people in the exposed state between the two regions by replacing Eq. (2) with

$$\dot{E}_i = (\beta_i S_i I_i - \alpha_i E_i) + \varepsilon_{ij} E_j - \varepsilon_{ji} E_i, \tag{6}$$

where $\varepsilon_{ii} = 0$ and $\varepsilon_{ij} \geqslant 0$ ($i \neq j$). Unlike the model of Flahault et al. [5], we omit the immigration of susceptible (healthy) residents. The exchange between S_1 and S_2 affects the transmission dynamics via changes in $\mathcal{R}_1(t)$ or $\mathcal{R}_2(t)$ only if the resultant change in S_1 or S_2 is a comparable order of N_i. This is not realistic in our context. Most of the migration between the cities is due to short-term trips. This is one reason why we do not include the exchange of S_i. Another reason is the difficulty of describing the individual visits in a closed form of differential equations. A reference to a past state, such as $S(t - T)$, appears for individuals who leave their home but return there after time T. The same problem arises for exposed individuals. However, the effect of their return on the dynamics of the epidemic is negligible since their number is much smaller than that of the city. Eq. (6) therefore accounts for the number of exposed individuals who depart but not those who return. The observed time course contains abrupt changes that are difficult to explain systematically. An additional stochastic process is needed in order to reproduce these changes. We considered two candidates for this stochastic process. The first candidate is to allow β_i to change with time. For example, we can consider a random walk process,

$$\ln \beta_i[t] = \ln \beta_i[t-1] + v_{\beta,i}, \quad v_{\beta,i} \sim \mathcal{N}(0, \sigma^2_{\beta,i}), \tag{7}$$

where the size of the random steps is controlled by an additional parameter $\sigma_{\beta,i}$. Letting the step be $\ln \beta_i$ instead of β_i guarantees that $\beta_i > 0$, as well as enabling β_i to change suddenly. This is reasonable approach since the observation profile and the recorded activities of the local governments suggest that the transmissibility was effectively reduced during the first wave in Kansai, and the epidemic died out locally. The second candidate is to retain the meanings of the categories and relationships of the SEIR model, but to make it fully stochastic. This is also reasonable since the number of reported patients is so small that the discrete and stochastic nature of the transmission events is significant. For example, Eq. (1) calculates that the proportion of susceptible individuals who become exposed during the time span Δt is $\beta(I_i/N_i)\Delta t$. If we regard this proportion as the transition probability, then the number of individuals who move from the susceptible to the exposed state follows a binomial process $B(\cdot|n = S, p = \beta(I_i/N_i)\Delta t)$. However, since p is very small, we instead use a Poisson process $\text{Poisson}(\cdot|\lambda = \beta(I_i/N_i)S\Delta t)$. If we assume that the other transitions also follow a Poisson process, we obtain a stochastic version of the SEIR model,

$$\Delta[E_i \to E_j]_t \sim \text{Poisson}(\cdot|E_{i,t-1}\varepsilon_{ij}\Delta t), \tag{8}$$
$$\Delta[S_i \to E_i]_t \sim \text{Poisson}(\cdot|\beta_i S_{i,t-1} I_{i,t-1}\Delta t), \tag{9}$$
$$\Delta[E_i \to I_i]_t \sim \text{Poisson}(\cdot|\alpha E_{i,t-1}\Delta t), \tag{10}$$
$$\Delta[I_i \to R_i]_t \sim \text{Poisson}(\cdot|\gamma I_{i,t-1}\Delta t), \tag{11}$$
$$S_{i,t} = S_{i,t-1} - \Delta[S_i \to E_i]_t, \tag{12}$$
$$E_{i,t} = E_{i,t-1} + \Delta[S_i \to E_i]_t - \Delta[E_i \to I_i]_t - \Delta[E_i \to E_j]_t + \Delta[E_j \to E_i]_t, \tag{13}$$
$$I_{i,t} = I_{i,t-1} + \Delta[E_i \to I_i]_t - \Delta[I_i \to R_i]_t, \tag{14}$$
$$R_{i,t} = R_{i,t-1} + \Delta[I_i \to R_i]_t, \tag{15}$$

with the time interval Δt set to be one day. We consider that the stochastic fluctuations in the events is more important and thus employ the second candidate. It should be noted that the model becomes excessively flexible if we incorporate both the stochastic variation of β_i and the stochastic realization of infectious events. This will be demonstrated in Section 3.3.

2.4. Model scoring and state estimation in the state-space model

When combined with a model (presented below) that relates the observed data J_i^{obs} to the simulation counterpart J_i, the simulation model discussed above can be cast as a *state-space model* (SSM), which we will fit using a standard particle filter algorithm [14,15].

Notation. We shall use the following notation to describe the state-space model and the particle filter algorithm:

- Vectors $\boldsymbol{x}$ and $\boldsymbol{\theta}$ are the aggregate simulation variables and the model parameters, respectively.

$$\boldsymbol{\varepsilon} = (\varepsilon_{12}, \varepsilon_{21}), \quad \boldsymbol{\beta} = (\beta_1, \beta_2),$$
$$\boldsymbol{\theta} = (\alpha, \gamma, \boldsymbol{\beta}, \boldsymbol{\varepsilon}),$$
$$\boldsymbol{x} = (S_1, E_1, I_1, R_1, J_1; S_2, E_2, I_2, R_2, J_2), \tag{16}$$

- A vector with a subscript, such as $\boldsymbol{x}_t$, denotes the value of $\boldsymbol{x}$ at the discrete time point t.
- $p(\boldsymbol{y}_t|\boldsymbol{x}_t, \boldsymbol{\theta})$ denotes the probability density function of $\boldsymbol{y}_t$ conditional on $\boldsymbol{x}_t$ and $\boldsymbol{\theta}$.
- A vector with a parenthesized superscript, such as $\boldsymbol{x}_t^{(m)}$, is a realization of a random number $\boldsymbol{x}_t$, where $\boldsymbol{x}_t^{(m)} \sim p(\cdot|\boldsymbol{y}_1, \ldots, \boldsymbol{y}_t)$ is used to denote the distribution from which the realizations have been sampled.

System and observation models. Our simulation model consists of Eqs. (8)–(15). Using the notation of Eq. (16), we find that this model is a special case of the stochastic map for $\boldsymbol{x}$,

$$\boldsymbol{x}_t = \boldsymbol{p}(\cdot|\boldsymbol{x}_{t-1}, \boldsymbol{\theta}). \tag{17}$$

This is called the *system model*, and it is the first part of the SSM.

We assume that the observed cases are the number of new infections, subject to some Poisson error. This assumption is described by

$$(J_{1,t}^{\text{obs}}, J_{2,t}^{\text{obs}}) \sim \prod_{i=1}^{2} \text{Poisson}(J_{i,t}^{\text{obs}}|J_{i,t}) \quad \text{with} \quad \text{Poisson}(y|m) = e^{-m}m^y/y!. \tag{18}$$

Setting $\boldsymbol{y} = (J_1^{\text{obs}}, J_2^{\text{obs}})$, we see that it is a special case of

$$\boldsymbol{y}_t \sim p(\cdot|\boldsymbol{x}_t, \boldsymbol{\theta}). \tag{19}$$

This is called the *observation model*, and it is the second part of the SSM.

Likelihood and state estimation. For a given configuration of the parameter $\boldsymbol{\theta}$ and an initial condition $\boldsymbol{x}_0$, the likelihood of the SSM with respect to the observed time-course data $(\boldsymbol{y}_1, \ldots, \boldsymbol{y}_T)$ is

$$\begin{aligned} L(\boldsymbol{x}_0, \boldsymbol{\theta}) &\equiv p(\boldsymbol{y}_T, \ldots, \boldsymbol{y}_1|\boldsymbol{x}_0, \boldsymbol{\theta}) \\ &= p(\boldsymbol{y}_T|\boldsymbol{y}_{T-1}, \ldots, \boldsymbol{y}_1, \boldsymbol{x}_0, \boldsymbol{\theta}) p(\boldsymbol{y}_{T-1}, \ldots, \boldsymbol{y}_1|\boldsymbol{x}_0, \boldsymbol{\theta}) \\ &= \cdots = \prod_{t=1}^{T} p(\boldsymbol{y}_t|\boldsymbol{y}_{t-1}, \ldots, \boldsymbol{y}_1, \boldsymbol{x}_0, \boldsymbol{\theta}) \\ &= \prod_{t=1}^{T} \int p(\boldsymbol{y}_t|\boldsymbol{x}_t, \theta) p(\boldsymbol{x}_t|\boldsymbol{y}_{t-1}, \ldots, \boldsymbol{y}_1, \boldsymbol{x}_0, \boldsymbol{\theta}) d\boldsymbol{x}_t, \end{aligned} \tag{20}$$

where we use the fact that $p(\boldsymbol{y}_t|\boldsymbol{x}_t, \boldsymbol{y}_{t-1}, \ldots, \boldsymbol{y}_1, \theta) = p(\boldsymbol{y}_t|\boldsymbol{x}_t, \theta)$ holds, by the Markov property of Eq. (19).

The estimation of state $\boldsymbol{x}_t$ is made from the conditional distribution of the state given the observation data up to some time point $t + \Lambda$, that is, $p(\boldsymbol{x}_t|\boldsymbol{y}_1, \ldots, \boldsymbol{y}_{t+\Lambda})$. The common conditioning variables $\boldsymbol{x}_0$ and $\boldsymbol{\theta}$ are dropped for the moment. This conditional distribution is called *predictive* (if $\Lambda < 0$), *filtered* ($\Lambda = 0$), or *smoothed* ($\Lambda > 0$). We will use the expectation of x_t later to smooth the distribution in order to represent the result of fitting it to the data, that is,

$$\hat{\boldsymbol{x}}_t = \int \boldsymbol{x}_t p(\boldsymbol{x}_t|\boldsymbol{y}_1, \ldots, \boldsymbol{y}_{t+\Lambda}) d\boldsymbol{x}_t, \tag{21}$$

where Λ is called the *lag*; Λ is the length of the future observations that are used for the state estimation. We set $\Lambda = 9$ based on the observation that the time-course profiles in Fig. 2 contain a variation in $J_i^{\text{obs}}[t]$ on the time scale of one week.

Particle filter. We used a particle filter (PF) to evaluate Eqs. (20) and (21). Only the outline of a standard algorithm is shown below. Details of the PF can be found in original research papers [16–18] or a book [19]. In a PF algorithm, a distribution $p(\boldsymbol{x}_t|\boldsymbol{y}_1, \ldots, \boldsymbol{y}_v)$ with some time point v is approximately represented by an ensemble $\{\boldsymbol{x}_t^{(m)}\}_{m=1}^{M}$ of realized values of $\boldsymbol{x}_t$, that is,

$$p(\boldsymbol{x}_t|\boldsymbol{y}_1, \ldots, \boldsymbol{y}_v) \cong \frac{1}{M}\sum_{m=1}^{M} \delta(\boldsymbol{x}_t - \boldsymbol{x}_t^{(m)}).$$

For simplicity, we will show below the procedure for the filter case ($\Lambda = 0$). With a little modification, the procedure can be used for smoother cases ($\Lambda > 0$) [17,19,20], as is shown in the Appendix.

Particle filter algorithm

1. Set the value of $\boldsymbol{\theta}$ and generate an ensemble $\{\boldsymbol{z}_0^{(m)}\}_{m=1}^{M}$ that represents the prior distribution $p(\boldsymbol{x}_0|\boldsymbol{\theta})$ of the initial condition $\boldsymbol{x}_0$.

2. Assume that the ensemble $\{\boldsymbol{x}_t^{(m)}\}_{m=1}^M$ is a representative sample from the predictive distribution $p(\boldsymbol{x}_t|\boldsymbol{y}_1,\ldots,\boldsymbol{y}_{t-1})$ and that the ensemble $\{\boldsymbol{z}_t^{(m)}\}_{m=1}^M$ is a representative sample from the filtered one $p(\boldsymbol{x}_t|\boldsymbol{y}_1,\ldots,\boldsymbol{y}_t)$. Then, the following steps construct $\{\boldsymbol{x}_t^{(m)}\}_{m=1}^M$ and $\{\boldsymbol{z}_t^{(m)}\}_{m=1}^M$ from $\{\boldsymbol{x}_{t-1}^{(m)}\}_{m=1}^M$ and $\{\boldsymbol{z}_{t-1}^{(m)}\}_{m=1}^M$.
   (a) For $m=1,\ldots,M$, draw $\boldsymbol{x}_t^{(m)}$ from $p(\boldsymbol{x}_t|\boldsymbol{x}_{t-1},\boldsymbol{\theta})$.
   (b) For $m=1,\ldots,M$, calculate the likelihood $l_t^{(m)}=p(\boldsymbol{y}_t|\boldsymbol{x}_t^{(m)},\boldsymbol{\theta})$.
   (c) For $m=1,\ldots,M$, calculate $w_t^{(m)}=l_t^{(m)}/\sum_{m=1}^M l_t^{(m)}$.
   (d) Resample from $\{\boldsymbol{x}_t^{(m)}\}_{m=1}^M$ with the probabilities $\{w_t^{(m)}\}_{m=1}^M$ to obtain $\{\boldsymbol{z}_t^{(m)}\}_{m=1}^M$.
   (e) Use the sample to evaluate the properties of the distribution $p(\boldsymbol{x}_t|\boldsymbol{y}_t,\ldots,\boldsymbol{y}_1)$. For example, Eq. (21) is evaluated by

$$\hat{\boldsymbol{x}}_t=\frac{1}{M}\sum_{m=1}^M \boldsymbol{z}_t^{(m)}. \tag{22}$$

3. Iterate Step 2 up to the last observation time. Then Eq. (20) is evaluated by

$$L(\boldsymbol{x}_0,\boldsymbol{\theta})\approx\frac{1}{M}\sum_{m=1}^M\prod_{t=1}^T l_t^{(m)}.$$

3. Model comparison

3.1. Scoring

The significance of immigration is evaluated by comparing the case of $\varepsilon_{ij}>0$ with the case of $\varepsilon_{ij}=0$. We introduce a score for the goodness of each setting as a function of ε_{12} and ε_{21}, by maximizing L for the rest of the parameters:

$$\mathrm{SCORE}(\varepsilon_{12},\varepsilon_{21})=-\max_{\theta\setminus\{\varepsilon\}}\ln L(\boldsymbol{x}_0,\boldsymbol{\theta}). \tag{23}$$

However, since it is difficult to maximize $L(x_0,\theta)$ over all (x_0,θ), we fix most of the parameters based on the knowledge of influenza and maximize L only over β_1. First, for the components of $\boldsymbol{\theta}$, we set $\alpha^{-1}=3.5$ [day] and $\gamma^{-1}=3.0$ [day], based on typical values of the incubation and infectious periods [21], respectively. In Kanto, the number of confirmed cases was basically monotonically increasing, and hence $\mathcal{R}_2>1$. We assigned an acceptable value [22–24], $\mathcal{R}_2=1.5$ and shall discuss below the effect of selecting different values. We further reduced the number of parameters by assuming $\varepsilon_{12}=\varepsilon_{21}=\varepsilon$. Second, for the components of $\boldsymbol{x}_0$, we considered that it is difficult to determine good values for $E_i(0)$ and $I_i(0)$, although their scales are roughly estimated by the observation data from the first several days (recall $J_i\approx\alpha_i E_i$). We thus assumed priors on these values according to a rough estimation and averaged their likelihood values. The priors are given by

$$\begin{aligned}&E_1(0),\quad I_1(0)\sim\mathcal{N}_{>0}(\cdot\,|\,\mu=125,\sigma^2=75^2),\\&E_2(0),\quad I_2(0)\sim\mathcal{N}_{>0}(\cdot\,|\,\mu=0,\sigma^2=5^2),\end{aligned} \tag{24}$$

where $\mathcal{N}_{>0}(x|\,\mu,\sigma^2)$ denotes the truncated normal distribution of x with domain $x>0$, mean μ, and variance σ^2. Here, $E_i(0)$ and $I_i(0)$ are assumed to be of similar scale, and $E_1(0)$ is estimated to be roughly 100 from $J_1^{\mathrm{obs}}(0)=38$ and $J_1^{\mathrm{obs}}(1)=67$, whereas $E_2(0)$ is assumed to be arbitrarily small, due to the absence of patients in Kanto at the beginning. Representative values of $E_i(0), I_i(0)$, and the other component of the initial condition are given by $\hat{x}_0$, which is defined by Eq. (21), and calculated with the particle-smoother algorithm.

In summary, the above treatments mean that we replace L with L^* in Eq. (23),

$$\begin{aligned}L^*(\varepsilon,\mathcal{R}_1,\mathcal{R}_2)=\frac{1}{M}\sum_{m=1}^M L\Big(&\varepsilon_{12}=\varepsilon_{21}=\varepsilon,\beta_1=\frac{\mathcal{R}_1}{\gamma},\beta_2=\frac{\mathcal{R}_2}{\gamma},\\&\alpha=\frac{1}{3.5},\gamma=\frac{1}{3};S_1=\frac{N_1\mathcal{R}_1}{\mathcal{R}_2},E_1^{(m)},I_1^{(m)},\mathcal{R}_1=0,\\&S_2=N_2,E_2^{(m)},I_2^{(m)},\mathcal{R}_2=0\Big),\end{aligned}$$

where $E_i^{(m)}$ and $I_i^{(m)}$ $(i=1,2,m=1,\ldots,M)$ are sampled from Eq. (24). For each $(\varepsilon,\mathcal{R}_1)$, L^* and the state estimation have been calculated using the filtering and smoother algorithms with $M=2,621,440(=32,768\times80)$ particles, respectively. It takes about 3 min for these calculations on an 80-way parallel processor.

3.2. Dependency of score on ε

The left panel of Fig. 3 shows the score as a function of ε and $\mathcal{R}_1(0)$. For any fixed ε, the score monotonically increases (improves) as $\mathcal{R}_1(0)$ increases, whereas the score becomes less sensitive to $\mathcal{R}_1(0)$ as the value of ε increases. The score is almost constant $\mathcal{R}_1(0)>1$ for each value of ε, and these constant values are similar between the values of ε. Therefore, we conclude that the observation data set we used does not support the significance of migration of infected patients between the two areas. This is also confirmed from the time course of J_i $(i=1,2)$ in the middle and right panels of Fig. 3, where the J_i components of $\dot{\boldsymbol{x}}$ given by Eq. (21) with $\Lambda=9$ are plotted for different values of ε. The differences from the observed J_i^{obs} (indicated by grey bars) is similar between the different values of ε.

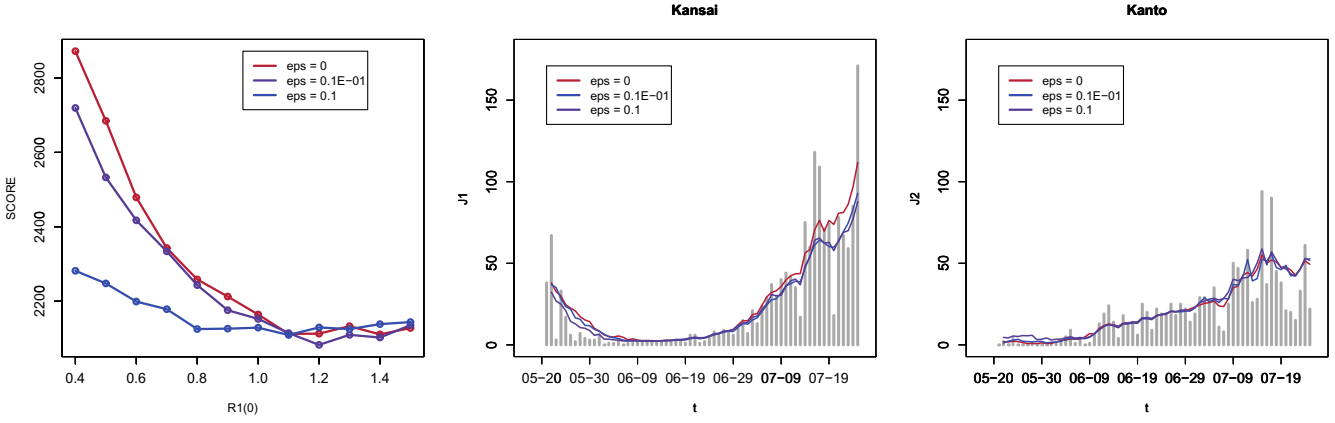

Fig. 3. Score as a function of $\mathcal{R}_1(0)$ for $\varepsilon_{12}=\varepsilon_{21}\equiv\varepsilon=0$, 0.01, and 0.1 (left panel). Time courses of smoothed distributions of J_i in Kansai (middle panel) and Kanto (right panel) corresponding to the best scores for respective values of ε.

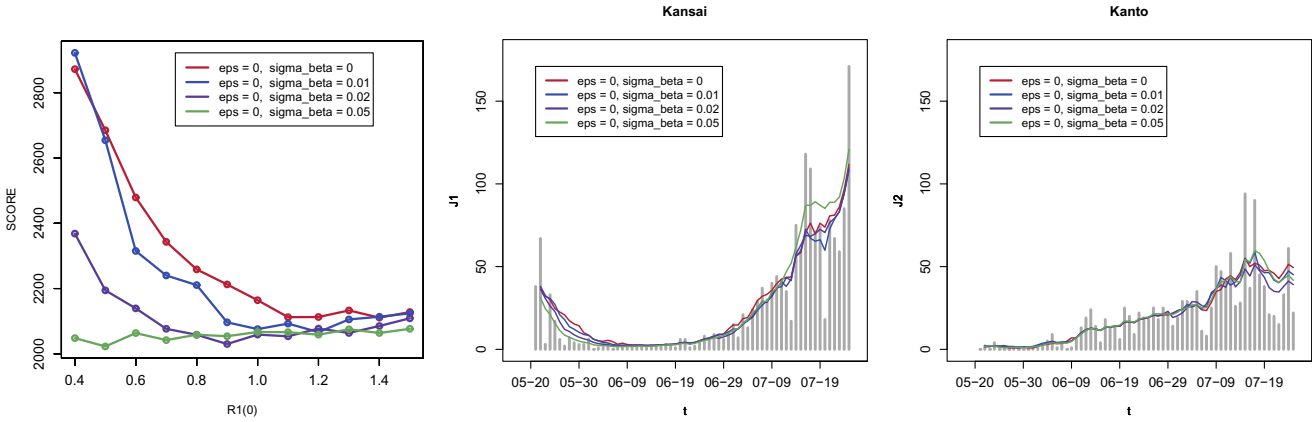

Fig. 4. Similar to Fig. 3, but the respective curves correspond to different values of $\sigma_{\beta,1} = \sigma_{\beta,2} = \sigma_\beta$ (β_i is the step size of the random walk). In all curves, $\varepsilon = 0$.

3.3. Discussion

We have not incorporated the stochastic time variation of β_i in our model. We now demonstrate what happens if we allow β_i to vary stochastically, as given by Eq. (7). This process retains the SSM formalism if we move β_i from $\boldsymbol{\theta}$ to $\boldsymbol{x}$ and add $\sigma_{\beta,i}$ to $\boldsymbol{\theta}$. For simplicity, we set $\sigma_{\beta,1} = \sigma_{\beta,2} \equiv \sigma_\beta$ and calculate how the score depends on $\mathcal{R}_1(0)$. The result for the case of $\varepsilon = 0$ shown in Fig. 4 indicates that the identifiability of $\mathcal{R}_1(0)$ weakens with increasing step size σ_β of the random walk. Although cases of nonzero σ_β yield better scores than the case of $\sigma_\beta = 0$, no meaningful difference is recognized during the time course of J_i.

The score was also evaluated for cases of smaller transmissibilities in Kanto: $\mathcal{R}_2(0) = 0.8$, 1.0, and 1.2. The results shown in Fig. 5 indicate that the effect of the immigration is less significant with a smaller $\mathcal{R}_2(0)$. In particular, a setting of $\epsilon = 0$ (decoupled two citis), $\mathcal{R}_1(0) > 1$ (increasing trend in Kansai in average) and $\mathcal{R}_2(0) < 0$ (increasing trend in Kanto in average) is acceptable, since the value of the likelihood closes to the best in Fig. 3. Due to a large uncertainty coming from a small number of patients, it is possible that the disease is transmitted much more frequently than the average and an increasing trend is realized in Kanto, whereas less frequently transmitted in Kansai and a gap between the first and the second waves appeared.

We have concluded that the significance of the exchange of infected individuals between these two cities cannot be verified from this data. It is, however, worth showing that this conclusion depends on the scale of the reported patients. We have carried out the same experiments and evaluated the likelihood but with a synthetic observation data of doubled confirmed cases. Comparing the smallest values of the score for the respective values of ε, we find that the case of $\varepsilon = 0.1$ is better than that of $\varepsilon = 0$.

4. Conclusion

We have studied the significance of migration between the Kanto and Kansai areas in the 2009 influenza pandemic in Japan. In order to perform a comparison based on the likelihood (precisely, the Akaike information criterion, AIC), we have employed two sets of the SEIR model coupled by the parameter ε, which describes the amount of migration between the two areas. Moreover, since the number of reported patients is too small to apply a continuous approximation, we assumed that both the transmission of infection and the recovery from the disease follow Poisson processes.

The values of the maximum likelihood for the respective values of ε were similar. Therefore, we conclude that the significance of migration is not verified with this data. This means that the multiple epidemic waves in Kansan were not necessarily caused by infected individuals entering from other areas, but they could have been caused by the stochastic nature of the infectious events. However, we note that with virtual data for which the number of patients was doubled, the likelihood of $\varepsilon = 0.1$ was better than that for $\varepsilon = 0$. Thus, when more patients are reported, due to a higher infection rate and/or to a higher detection rate, the method demonstrated in this paper can detect the effect of immigration.

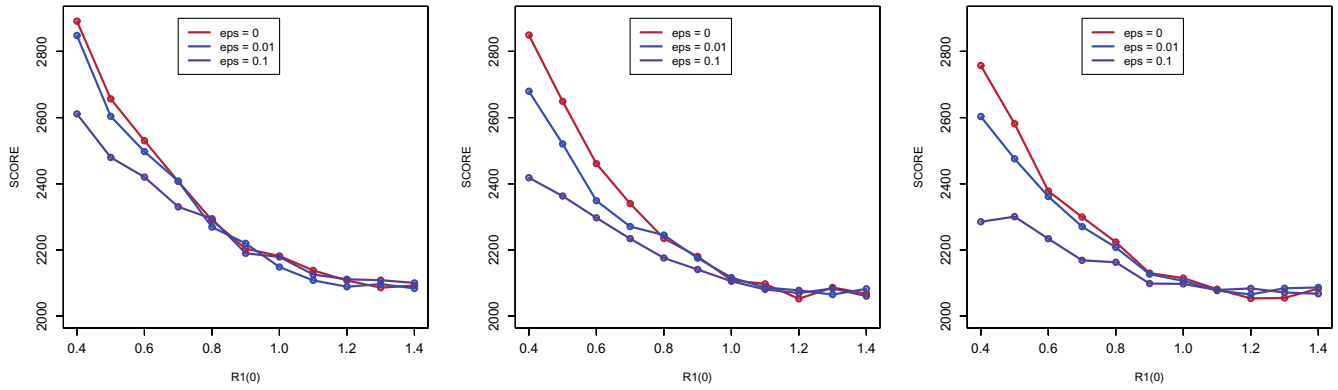

Fig. 5. Score as a function of $\mathcal{R}_1(0)$ for $\varepsilon_{12} = \varepsilon_{21} \equiv \varepsilon = 0$, 0.01, and 0.1, and for different values of $\mathcal{R}_2(0) = 0.8$, 1.0, and 1.2.

Appendix A. Smoother algorithm

We can apply the procedure of the PF algorithm in Section 2.4 to obtain a smoothed distribution $p(x_{t-\Lambda}|\boldsymbol{y}_1,\ldots,\boldsymbol{y}_t)$ for a fixed Λ-lag by defining a new SSM in the following way. Let us consider an augmented state vector $\tilde{\mathbf{x}}_t$ that includes the state vectors from the last Λ time-steps prior to the current step,

$$\tilde{\mathbf{x}}_t \equiv (\tilde{\mathbf{x}}_{0,t}, \tilde{\mathbf{x}}_{1,t}, \ldots, \tilde{\mathbf{x}}_{\Lambda,t}) \equiv (\mathbf{x}_t, \mathbf{x}_{t-1}, \ldots, \mathbf{x}_{t-\Lambda}).$$

We then define the SSM model for this augmented vector $\tilde{\mathbf{x}}_t$ so as to be consistent with Eqs. (17) and (19),

$$\tilde{\mathbf{x}}_{0,t} = \boldsymbol{f}(\tilde{\mathbf{x}}_{0,t-1}|\boldsymbol{\theta}) + \boldsymbol{v}_t, \quad \boldsymbol{v}_t \sim p(\boldsymbol{v}_t), \quad \tilde{\mathbf{x}}_{k,t} = \tilde{\mathbf{x}}_{k-1,t-1} \quad (k = 1,\ldots,\Lambda), \tag{A.1}$$

$$\boldsymbol{y}_t \sim p(\boldsymbol{y}_t|\tilde{\mathbf{x}}_{0,t}, \boldsymbol{\theta}). \tag{A.2}$$

Eq. (A.1) implies that $\tilde{\mathbf{x}}_t$ is constructed by updating $\boldsymbol{x}_{t-1}$ to obtain $\boldsymbol{x}_t$ with respect to the original system model Eq. (17) while keeping the past Λ states $\boldsymbol{x}_{t-1},\ldots,\boldsymbol{x}_{t-\Lambda}$ (Fig. 6). By applying the PF procedure to Eqs. (A.1) and (A.2), we have the following procedure for the smoother.

1. Set the value of $\boldsymbol{\theta}$ and generate an ensemble $\{\boldsymbol{z}_0^{(m)}\}_{m=1}^M$ that represents the prior distribution $p(\boldsymbol{x}_0|\boldsymbol{\theta})$ for the initial condition $\boldsymbol{x}_0$. Each member $\tilde{\mathbf{z}}_0^{(i)}$ in the ensemble of augmented state vectors is constructed by $\tilde{\mathbf{z}}_{0,0}^{(i)} = \boldsymbol{z}_0^{(i)}$, and $\tilde{\mathbf{z}}_{k,0}^{(i)} = \textit{undefined}$ $(k = 1,\ldots,\Lambda)$.
2. Assume that the ensemble $\{\tilde{\mathbf{x}}_t^{(m)}\}_{m=1}^M$ represents the predictive distribution $p(\tilde{\mathbf{x}}_t|\boldsymbol{y}_1,\ldots,\boldsymbol{y}_{t-1})$ and that the ensemble $\{\tilde{\mathbf{z}}_t^{(m)}\}_{m=1}^M$ represents that of the filtered distribution $p(\tilde{\mathbf{x}}_t^{(m)}|\boldsymbol{y}_1,\ldots,\boldsymbol{y}_t)$. Then, the following steps construct $\{\tilde{\mathbf{x}}_t^{(m)}\}_{m=1}^M$ and $\{\tilde{\mathbf{z}}_t^{(m)}\}_{m=1}^M$ from $\{\tilde{\mathbf{x}}_{t-1}^{(m)}\}_{m=1}^M$ and $\{\tilde{\mathbf{z}}_{t-1}^{(m)}\}_{m=1}^M$.
   (a) For $m = 1,\ldots,M$, draw $\boldsymbol{v}_t^{(m)} \sim p(\boldsymbol{v}_t)$, calculate $\tilde{\mathbf{x}}_{0,t}^{(m)} = \boldsymbol{f}(\tilde{\mathbf{z}}_{0,t-1}^{(m)}, \boldsymbol{v}_M^{(m)}|\boldsymbol{\theta})$, and copy $\tilde{\mathbf{x}}_{k-1,t-1}^{(m)} = \tilde{\mathbf{z}}_{k,t}^{(m)}$ $(k = 1,\ldots,\Lambda)$ to obtain $\{\tilde{\mathbf{x}}_t^{(m)}\}_{m=1}^M$.
   (b) For $m = 1,\ldots,M$, calculate the likelihood $l_t^{(m)} = p(\boldsymbol{y}_t|\tilde{\mathbf{x}}_t^{(m)}, \boldsymbol{\theta}) = p(\boldsymbol{y}_t|\tilde{\mathbf{x}}_{0,t}^{(m)}, \boldsymbol{\theta})$.
   (c) For $m = 1,\ldots,M$, calculate $w_t^{(m)} = l_t^{(m)} / \sum_{m=1}^M l_t^{(m)}$.
   (d) Resample from $\{\tilde{\mathbf{x}}_t^{(m)}\}_{m=1}^M$ with the probabilities $\{w_t^{(m)}\}_{m=1}^M$ to obtain $\{\tilde{\mathbf{z}}_t^{(m)}\}_{m=1}^M$.
   (e) For $m = 1,\ldots,M$, project $\tilde{\mathbf{z}}_t^{(m)}$ onto $\tilde{\mathbf{z}}_{\Lambda,t}^{(m)}$. The resulting ensemble $\{\boldsymbol{z}_{\Lambda,t}^{(m)}\}_{m=1}^M$ represents the smoothed distribution $p(\boldsymbol{x}_{t-\Lambda}|\boldsymbol{y}_t,\ldots,\boldsymbol{y}_1)$.

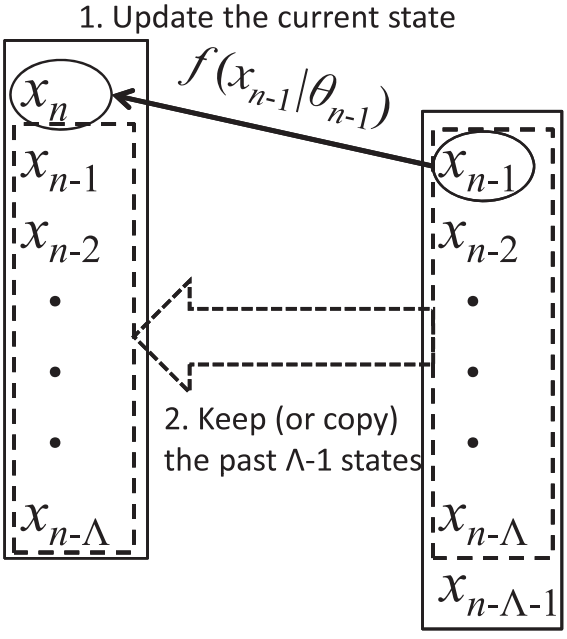

Fig. 6. Schematic illustration of the calculation of the extended system model.

Step 2(e) yields the ensemble for the smoothed distribution because

$$\begin{aligned} p(\boldsymbol{x}_{t-\Lambda}|\boldsymbol{y}_1,\ldots,\boldsymbol{y}_t) &= p(\tilde{\mathbf{x}}_{\Lambda,t}|\boldsymbol{y}_1,\ldots,\boldsymbol{y}_t) \\ &= \int p(\tilde{\mathbf{x}}_t|\boldsymbol{y}_1,\ldots,\boldsymbol{y}_t) d\tilde{\mathbf{x}}_{0,t}\ldots d\tilde{\mathbf{x}}_{\Lambda-1,t} \\ &\cong \int \frac{1}{M}\sum_{m=1}^M\prod_{k=0}^{\Lambda}\delta(\tilde{\mathbf{x}}_{k,t} - \boldsymbol{z}_{k,t}^{(m)}) d\tilde{\mathbf{x}}_{0,t}\ldots d\tilde{\mathbf{x}}_{\Lambda-1,t} \\ &= \frac{1}{M}\sum_{m=1}^M \delta(\tilde{\mathbf{x}}_{\Lambda,t} - \boldsymbol{z}_{\Lambda,t}^{(m)}). \end{aligned} \tag{A.3}$$

References

[1] H. Sato, H. Nakada, R. Yamaguchi, S. Imoto, S. Miyano, M. Kami, When should we intervene to control the 2009 influenza A(H1N1) pandemic, Euro Surveillance 15 (1) (2010). Available from: <http://www.eurosurveillance.org/ViewArticle.aspx?ArticleId=19455>.
[2] Infectious disease surveillance center, Pandemic (H1N1) 2009. Available from: <http://idsc.nih.go.jp/disease/swineinfluenzae/index.html>.
[3] Kobe City Public Health Center, Report on verification of measures against novel infulenza in Kobe City (in Japanese) (2011). Available from: <http://www.phcd.jp/shiryo/shininflu/H22hokenjogenbajoho1010kobecityHC2.pdf>.
[4] L.A. Rvachev, I.M. Longini, A mathematical model for the global spread of influenza, Mathematical Biosciences 75 (1985) 1.
[5] A. Flahault, S. Deguen, A.J. Valleron, A mathematical model for the European spread of influenza, European Journal of Epidemiology 10 (1994) 471.
[6] N.M. Ferguson, D.A.T. Cummings, S. Cauchemez, C. Fraser, S. Riley, A. Meeyai, S. Iamsirithaworn, D.S. Burke, Strategies for containing an emerging influenza pandemic in Southeast Asia, Nature 437 (2005) 209.
[7] I.M. Longini Jr., A. Nizam, S. Xu, K. Ungchusak, W. Hanshaoworakul, D.A.T. Cummings, M. Elizabeth Halloran, Containing pandemic influenza at the source, Science 309 (2005) 1084.
[8] S. Riley, Large-scale spatial-transmission models of infectious disease, Science 316 (2011) 1298.
[9] C. Wunsch, The Ocean Circulation Inverse Problem, Cambridge University Press, Cambridge, 1996.
[10] S. Tasaki, M. Nagasaki, M. Oyama, H. Hata, K. Ueno, R. Yoshida, T. Higuchi, S. Sugano, S. Miyano, Modeling and estimation of dynamic EGFR pathway by data assimilation approach using time series proteomic data, Genome Informatics 17 (2) (2006) 226.
[11] W.O. Kermack, A.G. McKendrick, Contributions to the mathematical theory of epidemics, Proceedings of the Royal Society of London Series A 115 (1927) 700.
[12] H.W. Hethcote, The mathematics of infectious diseases, SIAM Review 42 (2000) 599.
[13] H. Nishiura, H. Inaba, Prediction of infectious disease outbreak with particular emphasis on the statistical issues using transmission model, Proceedings of the Institute of Statistical Mathematics 54 (2) (2006) 461 (in Japanese).
[14] G. Kitagawa, W. Gersch, Smoothness Priors Analysis of Time Series, Springer-Verlag, New York, 1996.
[15] G. Kitagawa, Non-Gaussian state space modeling of nonstationary time series (with discussion), Journal of the American Statistical Association 79 (1987) 1032.
[16] N.J. Gordon, D.J. Salmond, A.F.M. Smith, Novel approach to nonlinear/non-Gaussian Bayesian state estimation, Radar and Signal Processing, IEE Proceedings-F 140 (2) (1993) 107.
[17] G. Kitagawa, Monte Carlo filter and smoother for non-Gaussian nonlinear state space models, Journal of Computational and Graphical Statistics 5 (1996) 1.
[18] T. Higuchi, G. Kitagawa, Knowledge discovery and self-organizing state space mode, IEICE Transactions on Information and Systems E83-D (1) (2000) 36–43.
[19] G. Kitagawa, S. Sato, Monte Carlo smoothing and self-organising state-space model, in: A. Doucet, N. de Freitas, N. Gordon (Eds.), Sequential Monte Carlo Methods in Practice, Springer, New York, 2001, p. 177.
[20] T.C. Clapp, S.J. Godsill, Fixed-lag smoothing using sequential importance sampling, in: J.M. Bernardo, J.O. Berger, A.P. Dawid, A.F.M. Smith (Eds.), Bayesian Statistics 6, Oxford University Press, Oxford, 1999, p. 744.
[21] F.S. Dawood, S. Jain, L. Finelli, M.W. Shaw, S. Lindstrom, R.J. Garten, et al., Emergence of a novel swine-origin influenza A (H1N1) virus in humans, The New England Journal of Medicine 360 (25) (2009) 2605.
[22] World Health Organization, Considerations for assessing the severity of an influenza pandemic, Weekly Epidemiological Record 84 (22) (2009) May 29

pp. 197–202. Available from: www.who.int/wer/2009/wer8422/en/index.html.

[23] H. Nishiura, C. Castillo-Chavez, M. Safan, G. Chowell, Transmission potential of the new influenza A(H1N1) virus and its age-specificity in Japan, Euro Surveillance 14 (22) (2009) (Available from: <http://www.eurosurveillance.org/ViewArticle.aspx?ArticleId=19227>).

[24] P.Y. Boëlle, P. Bernillon, J.C. Desenclos, A preliminary estimation of the reproduction ratio for new influenza A(H1N1) from the outbreak in Mexico, Euro Surveillance 14 (19) (2009) (Available from: <http://www.eurosurveillance.org/ViewArticle.aspx?ArticleId=19205>).